Article

Chinese Science Bulletin

Oceanology

September 2011 Vol.56 No.26: 2828–2838
doi: 10.1007/s11434-011-4619-4

Mineralogical and geochemical features of sulfide chimneys from the 49°39′E hydrothermal field on the Southwest Indian Ridge and their geological inferences

TAO ChunHui[1*], LI HuaiMing[1], HUANG Wei[2], HAN XiQiu[1], WU GuangHai[1], SU Xin[3], ZHOU Ning[4], LIN Jian[5], HE YongHua[1] & ZHOU JianPing[1]

[1] *Key Laboratory of Submarine Geosciences, Second Institute of Oceanography, State Oceanic Administration, Hangzhou 310012, China;*
[2] *Qingdao Institute of Marine Geology, Qingdao 266071, China;*
[3] *China University of Geosciences (Beijing), Beijing 100083, China;*
[4] *China Ocean Mineral Resources Research and Development Association, Beijing 100860, China;*
[5] *Woods Hole Oceanographic Institution, Woods Hole, MA 02543, USA*

Received January 14, 2011; accepted May 4, 2011

During January–May in 2007, the Chinese research cruise DY115-19 discovered an active hydrothermal field at 49°39′E/37°47′S on the ultraslow spreading Southwest Indian Ridge (SWIR). This was also the first active hydrothermal field found along an ultraslow-spreading ridge. We analyzed mineralogical, textural and geochemical compositions of the sulfide chimneys obtained from the 49°39′E field. Chimney samples show a concentric mineral zone around the fluid channel. The mineral assemblages of the interiors consist mainly of chalcopyrite, with pyrite and sphalerite as minor constitunets. In the intermediate portion, pyrite becomes the dominant mineral, with chalcopyrite and sphalerite as minor constitunets. For the outer wall, the majority of minerals are pyrite and sphalerite, with few chalcopyrite. Towards the outer margin of the chimney wall, the mineral grains become small and irregular in shape gradually, while minerals within interstices are abundant. These features are similar to those chimney edifices found on the East Pacific Rise and Mid-Atlantic Ridge. The average contents of Cu, Fe and Zn in our chimney samples were 2.83 wt%, 45.6 wt% and 3.28 wt%, respectively. The average Au and Ag contents were up to 2.0 ppm and 70.2 ppm respectively, higher than the massive sulfides from most hydrothermal fields along mid-ocean ridge. The rare earth elements geochemistry of the sulfide chimneys show a pattern distinctive from the sulfides recovered from typical hydrothermal fields along sediment-starved mid-ocean ridge, with the enrichment of light rare earth elements but the weak, mostly negative, Eu anomaly. This is attributed to the distinct mineralization environment or fluid compositions in this area.

sulfide chimneys, 49°39′E hydrothermal field, Southwest Indian Ridge, mid-ocean ridge, DY115-19 Chinese cruise

Citation: Tao C H, Li H M, Huang W, et al. Mineralogical and geochemical features of sulfide chimneys from the 49°39′E hydrothermal field on the Southwest Indian Ridge and their geological inferences. Chinese Sci Bull, 2011, 56: 2828–2838, doi: 10.1007/s11434-011-4619-4

In 1977 the first hydrothermal black smoker was discovered on the Galapagos Rift by scientists diving in a deep-sea submersible [1]. Since then, more than 170 hydrothermal fields have been found at different tectonic settings, such as the mid-ocean ridges, back-arc basins and intraplate volcanisms. Among them, more than 60% are distributed along mid-ocean ridges (MORs) [2]. By the end of last century, explorations of hydrothermal activities were mainly focused on the regions of the fast to intermediate spreading ridges in the Pacific Ocean and the slow spreading ridges in the Atlantic Ocean, few investigations along the ultraslow-spreading Southwest Indian ridge (SWIR) and the Gakkel Ridge in the Arctic [3].

The topographic, tectonic features and magmatic activities

*Corresponding author (email: taochunhuimail@163.com)

along mid-ocean ridges are controlled by the spreading rate [4,5]. The full spreading rate of the SWIR is about 1.3–1.6 cm/a [6], places SWIR in the category of ultraslow-spreading ridges with distinct topographic, tectonic, magmatic and hydrothermal features [7–11]. In recent years, geological and geophysical investigations on the SWIR have become a hot topic in the field of marine geology. However, reports on the hydrothermal activity are rare. During the Fuji cruise in 1997, hydrothermal plumes were found at six locations in the east of the SWIR. In 1998 relict hydrothermal field "Mt. Jourdanne" was located at 27°51′S/63°56′E during the Indoyo cruise. During R/V Knorr cruise 162 in 2000, eight sites with hydrothermal anomalies were discovered in the west of the SWIR [12,13], and in the next year, a hydrothermal deposits site in a peridotite-hosted field was discovered between 10° and 16°E [14]. However, active hydrothermal vents were not documented until 2007.

During January–May 2007, the Chinese research cruise DY115-19 discovered an active hydrothermal field at 49°39′E/37°47′S in the SWIR. This cruise was supported by the China Ocean Mineral Resources Research and Development Association (COMRA). The venting "black smoke" and biological communities were captured by the ABE (WHOI's autonomous benthic explorer) (Figure 1). Samples of chimneys and basalts as well as hydrothermal faunas were obtained by TVG (television video guided grab). This field is also the first active hydrothermal field found along any ultraslow-spreading ridges, which provides a good opportunity to understand the hydrothermal circulation, mineralization, vent biota and heat/mass contribution there. We presented results of the mineral assemblages and geochemical compositions of sulfide chimney samples obtained in the 49°39′E field.

1 Geological setting

The SWIR separates the African and Antarctic plates and extends from the east Rodriguez Triple Junction to the west Bouvet Triple Junction over a distance of about 8000 km, representing more than 10% of the total length of global ridges. It has a very slow spreading rate, and at some segments, spreading is oblique with respect to the direction of plate motion. The ridge axis is offset by sets of north-south trending transform faults, and is characterized by deep axial valleys and low magmatic budget [7]. Dick et al. [15]

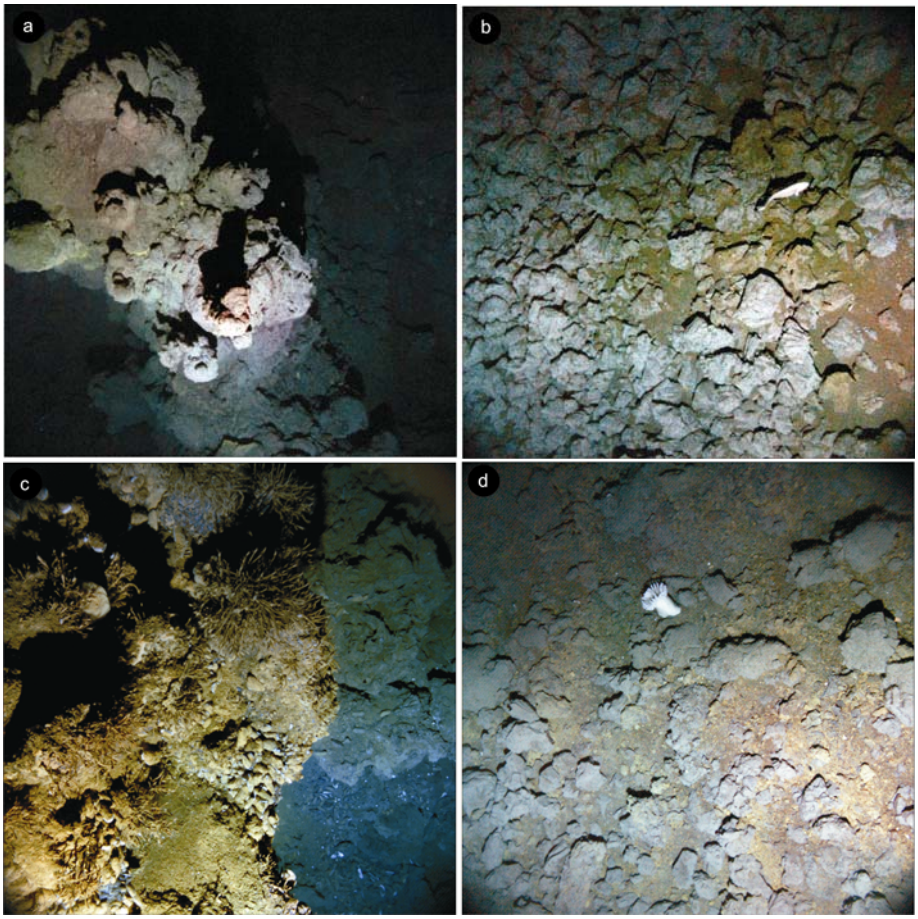

Figure 1 Seafloor in the study area. a, Sulfide chimney; b, altered basalt around the vent; c, stalked barnacles on the top of the vent; d, sea anemone. The photographs were taken by the ABE, WHOI's autonomous benthic explorer, during the cruise DY115-19. Views are 4 m×4 m.

suggested that the SWIR has the characters of both slow and ultraslow-spreading ocean ridges and is an example of a transitional ridge between slow and ultraslow. The crust is around 4 km thick, which is much thinner than the average thickness of the ocean crust (about 7 km [2]). However, the crustal thickness is not homogeneous at the SWIR. The plagioclase-hosted and olivine-hosted melt inclusions from the sections between 70°E and 49°E on the SWIR indicate the high melting fractions of mantle, shallow ridge axis depth and thick crust [16]. Cannat et al. [17] identified three types of seafloor at the SWIR as volcanic seafloor, smooth seafloor and corrugated seafloor. Among these, smooth terrain appears specific to ultraslow-spreading ridges and the mode of seafloor spreading may be analogous to processes at the ocean-continent transition of continental margins. The rocks exposed on the seafloor are mainly basalts, with some gabbros, pyroxenites and serpentinized peridotites [12]. Sauter et al. [18,19] and Cannat et al. [20] discussed the melt supply processes based on gravitational, magnetic and petrological data. They found that at the ultraslow-spreading ridges, the melt may migrate horizontally along the axis and mantle upwelling may be focus at some specific sections [18–20]. Moreover, the ridge spreading and hydrothermal activities may interact with hot spots such as the Marion, Bouvet, Del Cano and Crozet plateau [21,22].

The 49°39′E hydrothermal field is located at the west end of the east-west trending segment 28 of the SWIR between Indomed and Gallieni FZ (Figure 2). The axial depth along this segment varies from 1500 m at the southern end to 2800 m at the northern. Crustal thickness is up to 9 km [23], much thicker than in the vicinity (61°–63°E) where is about 4–5 km [24]. This implies that melt supply is abundant at this segment and magma provides enough heat for the hydrothermal activity. The seafloor surrounding the hydrothermal field is a dramatic relief, with a great deal of steep slope and lack of sediments. The vent is located at a high mound on the south-east wall of the ridge valley, at a depth of 2755 m. It is the junction point of the ridge valley and a small transform fault with local fissures.

2 Samples and methods

Two sulfide chimney samples, TVG4-1 and TVG4-2 (Figure 3), were analyzed. Sample TVG4-1 is a chunk of chimney edifice in irregular shape (about 22 cm in length and 10 cm in average width) with clear channel in the central part. The inner zone is dark gray and dense and the outer zone is porous. Concentric layers surrounding the feeder channel can be clearly observed on the cross or vertical profile. The out surface is covered by brown or black materials as a result of iron-hydroxidation. Sample TVG4-2 is a piece of dark gray sulfide crust with tiny fluid pores on the surface. Its inner part is denser than the outer.

Polished sections were prepared for petrographic examination. 11 subsamples were taken from the inner to outer portion along a profile across the chimney and they were named as 4-1-1 to 4-1-11 (Figure 3). Minerals of these subsamples were identified by Rigaku D/MAX 2400 X-ray diffraction (XRD) at the Institute of Geology and Geophysics, Chinese Academy of Sciences, Beijing. The major and minor elements were analyzed at the Quality Supervision and Testing Center of Exploration Geochemistry, Ministry of Land and Resources, Langfang, and the State Key Laboratory of Ore Deposit Geochemistry, Institute of Geochemistry, Chinese Academy of Sciences, Guiyang. Ag, Cu, Mo, Ni, Pb, Sb, Zn, U and Rare Earth Elements (REEs) were quantified by Inductively Coupled Plasma Mass Spectrometry

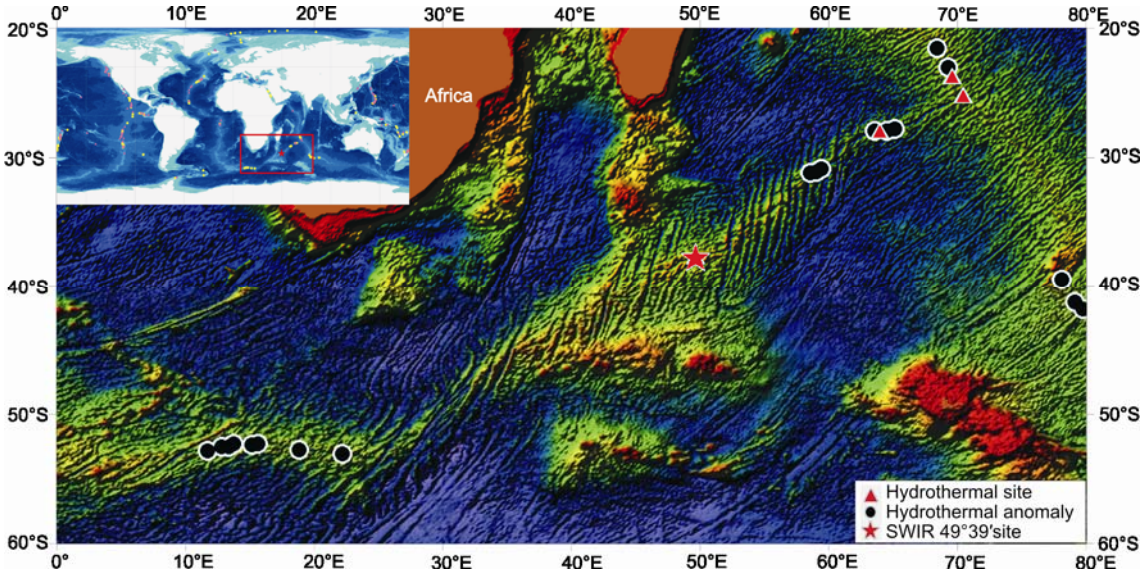

Figure 2 Location of the 49°39′E hydrothermal field (data from Baker et al. [10] and China Ocean Cruise).

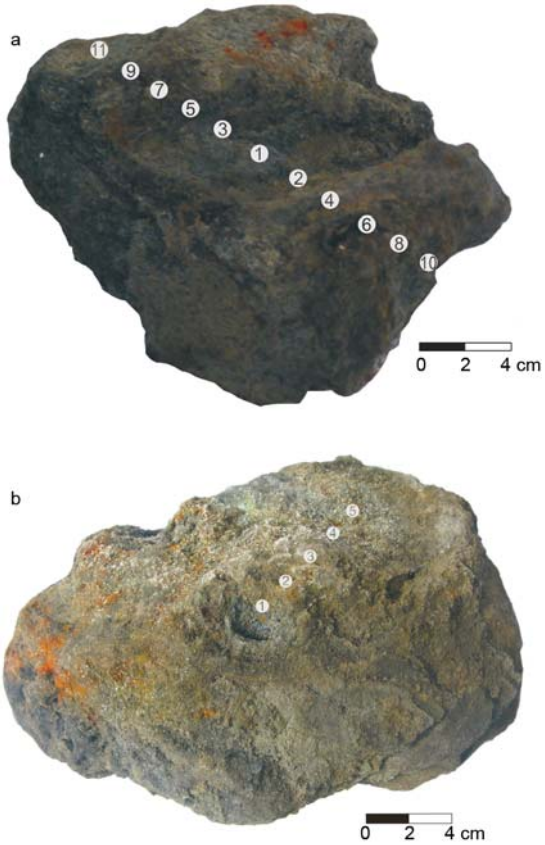

Figure 3 Pictures of sulfide chimney samples. a, TVG4-1; b, TVG4-2.

(ICP-MS). Fe and Al were determined by Inductively Coupled Plasma Optical Emission Spectrometry (ICP-OES). Si and Au were determined by X-ray Fluorescence (XRF) and Flameless Atomic Absorption Spectrometry (AAS), respectively.

3 Results and discussion

3.1 Mineralogy and textures

Early studies suggested that mineral paragenesis and textures are important to identify multiple stages of mineralization and understand the evolution of chimney edifices [25]. Typical models for the growth of sulfide chimneys have been described for several submarine hydrothermal fields. When the hot, acidic and Ca-rich hydrothermal fluids emanating from the vents react with cold SO_4^{2-}-rich seawater, sulfates, particularly anhydrite are precipitated (as well as sulfides like pyrrhotite, colloid from pyrite and marcasite) in marginal portions of the edifices. The new formed anhydrite walls restrict the seawater mixing with the hot fluid. Then chalcopyrite, pyrite and sphalerite precipitated at higher temperatures (>250°C), often being confined to the central portions of the chimneys [26–29]. With the growth of the chimneys, the temperature in the outer portion of the edifices decreases. When it is low enough, anhydrite begins to dissolve and the chimneys will collapse.

Mineral composition obtained by XRD and petrographic textures (Figures 4 and 5) show concentric mineral zones around the fluid channel in the samples TVG4-1 and TVG4-2. The interior of the chimney walls consist mainly of chalcopyrite, with a few of pyrite and sphalerite. Towards the intermediate portion, pyrite becomes the dominant mineral, with chalcopyrite and sphalerite becoming minor minerals. For the outer wall, the main sulfides are pyrite and sphalerite, with chalcopyrite as the minor minerals. Towards the outer margin of chimney wall, the mineral grains also become small and irregular in form. In addition, interstices among the minerals become abundant. Sporadically, fine and irregular barite and amorphous silica occur within interstices of the major minerals, such as pyrite and chalcopyrite. According to the chimney-growth model provided by Graham et al. [30], the mineral assemblages found in sample TVG-4 reflect the high maturity of its source chimney and hydrothermal field.

From microscopic observation of the polished optical sections of sample TVG4-1 (Figure 5), fine grain (usually <0.05 mm) texture was observed, and the grains are crystals

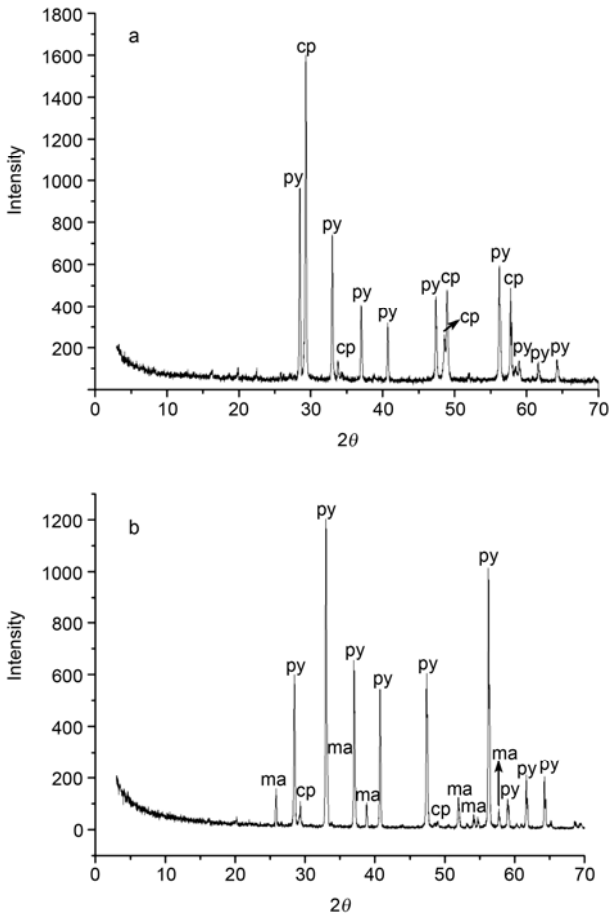

Figure 4 X-ray diffraction patterns for the two samples collected from the sulfide chimney. a, TVG4-1-1; b, TVG4-1-11. py, Pyrite; ma, marcasite; cp, chalcopyrite.

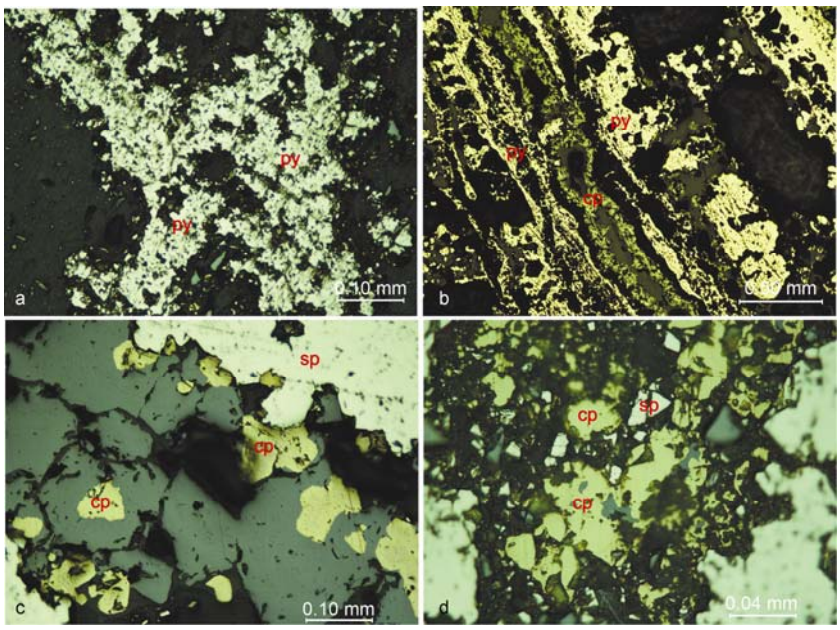

Figure 5 Textural features of sulfide chimney samples. py, Pyrite; cp, chalcopyrite; sp, sphalerite.

of pyrite, chalcopyrite and sphalerite in subhedral and xenomorphic unequigranular crystal forms. Pyrite is the most abundant mineral and as the main framework of the samples. Several pyrite crystals, anhedral, subhedral, euhedral cubic crystals, are present, arranged in irregular lines or dendritic clusters (Figure 5a). Chalcopyrite occurs as the dominant mineral only in the interior wall, while in the middle and outer part of the chimney, chalcopyrite and sphalerite occur irregularly within the inter-grain spaces of pyrite. Replacement of chalcopyrite by sphalerite, or on the contrast, are common, and remnants of such replacement were identified (Figure 5c,d). Thin pyrite laminars or layers were also observed under the microscope (Figure 5b) and very slim chalcopyrite layers occasionally fulfilled the fissure of pyrite layers.

3.2 Geochemistry

Major and minor compositions of the bulk analyses of samples TVG4-1 and TVG4-2 are presented in Table 1.

Because of the different tectonic settings, base rocks and fluid compositions, the sulfide chimneys recovered from different hydrothermal fields demonstrate different mineralogical and geochemical features. Seven other hydrothermal fields, including the TAG and Logatchev fields on the Mid-Atalntic Ridge (MAR), the 21°N and 7°24′S field on the East Pacific Rise (EPR), the MESO field on the Central Indian Ridge (CIR), the Mt. Jourdanne field on the SWIR and the Jade field in the Okinawa Trough were selected for comparison (Table 2). The chimney samples in this study contain high Fe concentrations (average 45.6 wt%) and generally low Cu and Zn contents (averages 2.83 wt% and 3.28 wt%, respectively), which are similar to the chimneys from other hydrothermal fields and indicating promising resource potential. The noble metals, Au and Ag, average contents are 2.0 ppm and 70.2 ppm, respectively, higher than those found in typical sediment-starved hydrothermal fields along mid-ocean ridges such as the MESO field on the CIR, the 7°24′S field on the EPR, and the TAG field on the MAR. However, they are similar to those found in the Mt. Jourdanne field on the SWIR, and lower than the Jade field in the back-arc basin Okinawa Trough. The high precious metal concentrations of the 49°39′E and the Mt. Jourdanne field on the SWIR may be a characteristic feature of metalliferous sulfide deposits on ultraslow-spreading ridge.

The sample TVG4-1 was selected for a detailed study of the growth process of the chimneys. The elements measured were divided into three groups according to the gradient of elemental contents from the interior to the outer portion. The first group, without an evident gradient, includes Fe, Cr, Ni, Sb, As and Mo. The second group consists of Zn, Pb, Cd, Au, Ag and U with an increasing trend of concentrations moving outwards. The elements Cu and Co with high contents in the interior and low on the outer surface were the third group (Figure 6).

The positive correlation between Cr, Ni and Fe ($r=0.87$ and 0.80; $n=11$) indicates that Cr and Ni occur in the pyrite crystals or other minerals associated with pyrite. The all values of correlation coefficients for Sb, As, Mo with Fe or Cu were all lower than 0.3, which indicates that these elements may disperse in the sulfide samples. Si has a significant negative correlation with Fe ($r=-0.95$; $n=11$). There are significant positive correlations among Zn, Pb, Cd, Au and Ag. These elements generally enrich in the outer portions of the chimney wall because their source minerals, such as sphalerite and galena, often precipitate at relatively

Table 1 Bulk geochemical compositions of sulfide chimney samples

		Fe_2O_3 (wt%)	Cu (wt%)	Zn (wt%)	Al_2O_3 (wt%)	SiO_2 (wt%)	Au (ppm)	Ag (ppm)	As (ppm)	Cd (ppm)	Co (ppm)	Cr (ppm)	Mo (ppm)	Ni (ppm)	Pb (ppm)	Sb (ppm)	U (ppm)
TVG4-1 pyrite-chalcopyrite																	
Inner	TVG4-1-1	51.5	5.82	2.15	0.47	0.92	1.8	55.8	87.5	81.4	234.2	4.0	35.3	2.0	53.5	3.35	0.34
	TVG4-1-2	37.0	1.11	1.05	1.10	4.70	0.8	24.6	77.7	56.0	198.6	5.1	14.5	0.6	48.6	2.88	0.06
	TVG4-1-3	56.4	0.75	0.38	0.24	0.58	1.6	15.6	89.0	11.2	413.7	9.0	19.1	3.3	72.0	3.40	0.26
	TVG4-1-4	56.4	2.06	0.61	0.28	1.38	1.0	25.7	91.0	19.9	227.7	11.4	22.3	2.8	85.5	4.15	0.23
(2 cm interval)	TVG4-1-5	39.9	0.54	0.40	0.72	3.42	0.8	14.4	60.1	16.7	176.4	4.8	13.8	1.6	58.6	3.04	0.01
	TVG4-1-6	40.5	0.44	0.35	0.45	3.15	0.5	12.3	66.5	13.3	231.9	4.1	17.8	0.3	96.6	3.12	0.01
	TVG4-1-7	55.9	0.68	0.32	0.23	0.78	1.0	13.9	92.5	7.5	263.5	14.1	21.6	4.6	106.0	3.05	0.32
	TVG4-1-8	49.8	0.77	9.29	0.22	–	3.9	122.6	86.5	315.9	105.0	8.6	25.6	3.7	183.0	9.15	0.49
	TVG4-1-9	52.3	0.22	7.86	0.14	1.98	2.4	115.6	36.0	182.7	63.5	13.0	43.2	3.7	213.5	3.40	1.10
Outer	TVG4-1-10	37.1	0.42	2.53	0.58	5.25	2.4	56.0	65.0	144.6	73.9	3.9	13.2	0.3	86.7	3.92	0.61
	TVG4-1-11	35.6	0.48	4.66	0.45	4.96	2.0	97.4	62.7	214.9	52.3	3.2	26.6	0.9	155.3	4.42	0.66
	Average	46.6	1.21	2.69	0.44	2.71	1.7	50.4	74.0	96.7	185.5	7.4	23.0	2.2	105.4	4.00	0.37
TVG4-2 pyrite-chalcopyrite																	
	TVG4-2-1	39.7	17.13	0.97	0.29	1.83	0.9	66.0	12.5	29.9	194.3	2.3	19.6	2.2	46.8	2.10	0.09
	TVG4-2-2	47.4	2.78	3.90	0.30	3.39	1.5	62.6	79.5	114.0	568.8	2.6	24.2	3.1	148.2	2.64	0.21
(2 cm interval)	TVG4-2-3	43.1	3.37	6.09	0.43	2.54	2.9	121.9	95.2	187.2	232.8	2.6	24.2	2.7	181.2	3.89	0.27
Inner	TVG4-2-4	42.6	3.69	6.49	0.41	1.81	3.9	143.1	75.2	209.1	154.3	2.5	27.7	1.7	155.3	3.95	0.20
	TVG4-2-5	45.8	2.05	4.39	0.27	0.76	3.5	139.0	56.8	148.5	294.1	3.3	61.9	4.1	184.6	3.25	0.97
	Average	43.7	5.80	4.37	0.34	2.07	2.5	106.5	63.8	137.7	288.9	2.7	31.5	2.8	143.2	3.17	0.35
Outer	Average	45.6	2.83	3.28	0.41	2.47	2.0	70.2	70.4	111.2	222.0	5.7	26.0	2.4	118.7	3.70	0.36

"–" Not detected.

Table 2 Comparison of major elemental compositions of sulfide from selected hydrothermal fields

	Waterdepth (m)	Spreading half-rate (cm/a)	Mineral-ogy	Cu (wt%)	Fe (wt%)	Zn (wt%)	Pb (wt%)	Au (ppm)	Ag (ppm)	Co (ppm)	Ni (ppm)	Cd (ppm)	Mo (ppm)	Data sources
Southwest Indian Ocean														
Study area	2750	0.6	py	2.83	45.6	3.28	0.01	2.0	70.2	222.0	2.4	111.2	26.0	this article
Mt. Jourdanne field	2940	0.7	sph	2.72	13.88	25.66	1.65	5.6	1021	–	7.67	1204	–	[13]
Central Indian Ocean														
MESO zone	2850	2.5	py, cp	29.4	27.6	0.5	0.03	0.7	55.3	583.7	127.8	23.5	300.0	[25]
			py, mc	6.2	37.2	0.8	0.05	0.6	22.4	1089.6	70.4	34.2	156.2	[25]
Pacific														
21°N, EPR	2600	3.0	chimney	0.2	2.0	1.1	0.05	<0.1	6.0	29.2	2.2	40.0	1.0	[25]
7°24′S, EPR	2740	7.7	sph, py	1.1	22.0	31.0	0.18	<0.2	118.0	4.1	4.1	840.0	45.0	[25]
			py	0.33	40.34	2.85	0.083	0.043	40	214	38	73	22	[38]
			py, cp	10.53	34.46	2.23	0.034	0.051	23.41	906	29	88	120	[38]
Atlantic														
TAG, MAR	3620	1.3	chimney	13.4	21.2	0.6	0.01	0.5	13.0	531.0	48.0	17.0	118.0	[25]
Logatchev, MAR	2600–3400	1.3	py, cp	12.8	37.3	1.4	0.02	1.4	38.0	75.0	–	38.0	144.0	[25]
			chimney	23.1	28.6	7.85	0.022	–	–	778	<20	–	–	[39]
Okinawa Trough														
Jade site	1340		sph, cp	4.41	11.50	27.4	12.00	8.60	11300	–	–	1300	–	[40]
				5.39	10.20	33.6	4.3	0.41	4100	–	–	2000	–	[40]

"–" Not detected; Py, pyrite; sph, sphalerite; cp, chalcopyrite; mc, marcasite.

low temperatures during the late or the waning stage of hydrothermal activity. According to Münch et al., the significant positive correlations of Cd, Au, Ag with Pb in the sulfides from the Mt. Jourdanne field can be attributed to remobilization under lower temperature conditions, possibly less than 100°C [13]. U is also rich in the outer margin section (up to 1.1 ppm). Because the content of U in the seawater (about 3.3 ppm), is much higher than that of hydrothermal fluid, the element U in the outer margin of chimney wall may mainly come from the seawater. The interior portions of chimneys are characterized by high Cu concentrations because they mainly consist of chalcopyrite, a mineral phase precipitating under higher temperature conditions. The correlation coefficients for Co with Cu is 0.24 ($n=11$). According to Hekinian and Fouquet, a partial enrichment in Co can be attributed to late-stage leaching of Fe from Co-bearing pyrite, thus relatively concentrating residual Co [31]. The enrichment of Co in the interior of our chimney samples may be caused by similar processes, but not by precipitation of chalcopyrite.

3.3 REEs

The REE geochemistry of metalliferous sulfides is generally considered as an indicator for the source and evolution processes of hydrothermal fluids. The REE concentrations and corresponding parameters for 16 subsamples from chimney samples TVG4-1 and TVG4-2 are presented in Table 3. There are some similarities between the REE geochemistry of samples TVG4-1 and TVG4-2. The REE concentrations (ΣREE) are low in both samples, varying between 0.2 and 3.66 ppm. ΣREE generally increase in profiles across the chimney wall from the dense interior portions to the loose outer ones, reflecting the different mixing proportions of the hydrothermal fluid with seawater [32]. The ratios of light rare earth elements (LREEs) to heavy rare earth elements (HREEs) vary between 1.29 and 6.46, showing the enrichment of LREEs. The chondrite-normalized patterns also show LREEs enrichment (Figure 7), with the variable $(La/Yb)_N$ 3.17 and 24.80. $(La/Sm)_N$ and $(Gd/Yb)_N$ vary between 2.03 and 7.04 and between 0.54 and 2.31,

Table 3 REE concentrations (ppm) of metalliferous sulfide chimney samples

	1-1	1-2	1-3	1-4	1-5	1-6	1-7	1-8	1-9	1-10	1-11	2-1	2-2	2-3	2-4	2-5	Average
La	0.260	0.136	0.250	0.515	0.154	0.109	0.235	0.395	0.610	0.130	0.108	0.038	0.034	0.095	0.054	0.081	0.200
Ce	0.550	0.286	0.450	1.050	0.237	0.221	0.650	0.950	1.550	0.252	0.196	0.067	0.069	0.273	0.157	0.230	0.449
Pr	0.050	0.050	0.055	0.080	0.032	0.029	0.165	0.070	0.130	0.035	0.024	0.008	0.008	0.018	0.014	0.019	0.049
Nd	0.200	0.101	0.205	0.255	0.108	0.087	0.550	0.240	0.525	0.117	0.089	0.039	0.030	0.060	0.047	0.067	0.170
Sm	0.056	0.025	0.047	0.046	0.031	0.019	0.055	0.041	0.097	0.027	0.021	0.009	0.008	0.018	0.013	0.025	0.034
Eu	0.011	0.007	0.010	0.011	0.006	0.006	0.008	0.009	0.042	0.007	0.006	0.003	0.002	0.003	0.003	0.006	0.009
Gd	0.029	0.020	0.041	0.040	0.023	0.017	0.035	0.035	0.092	0.022	0.022	0.004	0.005	0.011	0.004	0.012	0.026
Tb	0.006	0.003	0.006	0.006	0.004	0.003	0.008	0.005	0.013	0.003	0.005	0.003	0.001	0.002	0.001	0.002	0.004
Dy	0.035	0.023	0.039	0.029	0.022	0.022	0.045	0.026	0.068	0.020	0.030	0.008	0.004	0.014	0.005	0.011	0.025
Ho	0.007	0.004	0.006	0.005	0.006	0.004	0.007	0.005	0.013	0.006	0.008	0.001	0.001	0.003	0.002	0.003	0.005
Er	0.022	0.016	0.018	0.023	0.014	0.014	0.015	0.022	0.063	0.013	0.022	0.003	0.004	0.009	0.003	0.008	0.017
Tm	0.004	0.002	0.003	0.003	0.002	0.002	0.004	0.003	0.005	0.002	0.003	0.003	0.001	0.002	0.001	0.002	0.003
Yb	0.018	0.015	0.016	0.014	0.013	0.014	0.021	0.015	0.044	0.015	0.023	0.003	0.006	0.007	0.006	0.010	0.015
Lu	0.004	0.002	0.004	0.003	0.001	0.013	0.005	0.003	0.007	0.002	0.004	0.003	0.001	0.003	0.001	0.003	0.004
Y	0.235	0.164	0.240	0.180	0.155	0.138	0.225	0.155	0.400	0.156	0.228	0.023	0.029	0.100	0.049	0.086	0.160
LREE	1.127	0.605	1.017	1.957	0.568	0.471	1.663	1.705	2.954	0.568	0.444	0.162	0.151	0.467	0.288	0.427	0.911
HREE	0.360	0.249	0.373	0.303	0.240	0.227	0.365	0.269	0.705	0.239	0.345	0.049	0.052	0.151	0.072	0.135	0.258
LREE/HREE	3.13	2.43	2.73	6.46	2.37	2.07	4.56	6.34	4.19	2.38	1.29	3.33	2.90	3.09	4.00	3.16	
ΣREE	1.49	0.85	1.39	2.26	0.81	0.70	2.03	1.97	3.66	0.81	0.79	0.21	0.20	0.62	0.36	0.56	
δEu	0.83	0.96	0.70	0.78	0.69	1.02	0.56	0.73	1.36	0.88	0.85	1.40	0.97	0.65	1.27	1.06	
δCe	1.16	0.83	0.92	1.25	0.81	0.95	0.79	1.38	1.32	0.90	0.93	0.96	1.01	1.59	1.37	1.43	
$(La/Yb)_N$	9.74	6.11	10.53	24.80	7.99	5.25	7.54	17.75	9.35	5.84	3.17	10.11	3.82	9.15	6.07	5.71	
$(La/Sm)_N$	2.92	3.42	3.35	7.04	3.12	3.61	2.69	6.06	3.96	3.03	3.24	2.78	2.67	3.32	2.61	2.03	
$(Gd/Yb)_N$	1.30	1.08	2.07	2.31	1.43	0.98	1.34	1.88	1.69	1.18	0.77	1.13	0.67	1.27	0.54	1.02	

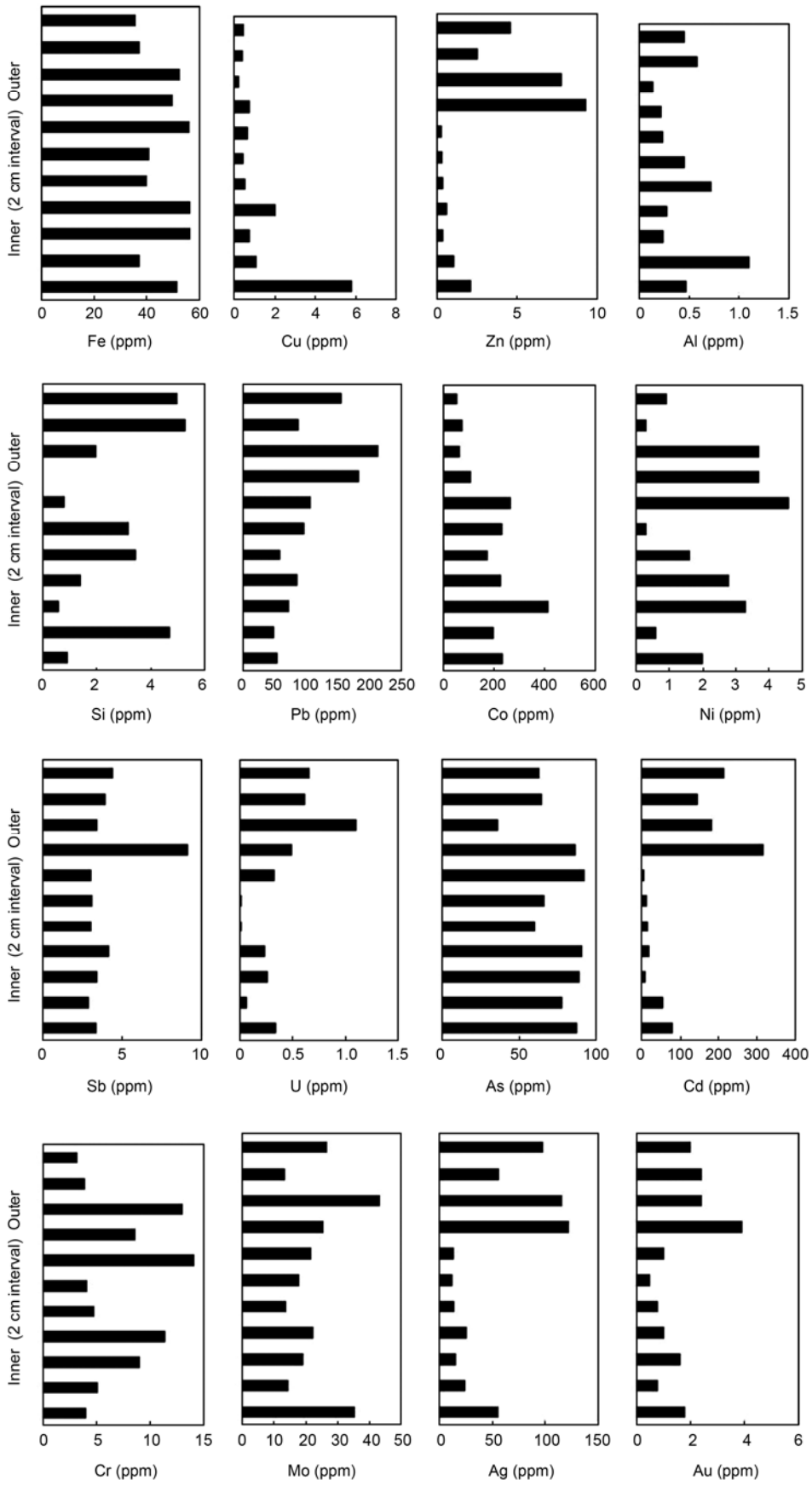

Figure 6 Variation in geochemical composition of sulfide chimney samples across the chimney wall.

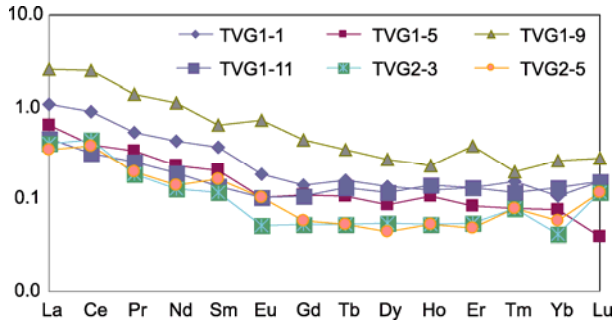

Figure 7 REE abundance patterns normalized to chondrite for some sulfide chimney samples. The chondritic REE values are given by Boynton (1984).

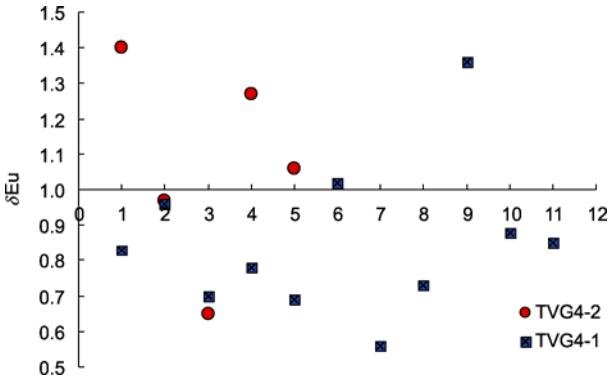

Figure 8 Varying patterns of δEu from TVG4-1 and TVG4-2.

respectively, indicating the higher degree fractionation among the LREEs than among the HREEs.

The pattern of LREEs enrichment with significant positive Eu anomalies is common for the hydrothermal fluids from the vent fields hosted on a basaltic or ultramafic rock substratum along MORs [33–35]. REEs in the sulfides mainly come from the fluids and thus inherit the patterns of the fluids. The sulfide samples show similar LREEs enrichment patterns, but with weakly negative anomalies for most samples (δEu: 0.56–1.40), which is different from the typical pattern found on the sediment-starved ridge. At present, our knowledge about the hydrothermal activities on the ultraslow-spreading ridges is still very poor and fluid samples were not available in the study area. In this article we have suggested some possible processes to interpret the REEs pattern found in the sulfides of the study area, based on the limited information.

Firstly, if the REE compositions of the hydrothermal fluid at the 49°39′E field is similar to those of typical venting fluids with the pattern of LREEs enrichment and a positive Eu anomaly, depositional environment and processes should be the main factors to control the pattern of sulfides. Except for Eu and Ce, other REEs usually occur as trivalent cations. Eu mainly occurs as a divalent cation under the conditions of high temperatures (>250°C), high pressure and low oxidation state. However, under lower temperature conditions, it can occur as both divalent and trivalent cations. Therefore, under the high temperature conditions in the hydrothermal fluids, the larger ion radius of Eu^{2+} (1.09) compared with Eu^{3+} (0.95) and the other trivalent REEs will restrict its entry into the precipitating sulfide crystals. This results in the negative Eu anomalies in the REE pattern. Evidences for this can often be found in the regular variations in Eu anomalies in the sulfides precipitated at different growth stages of chimneys under different temperature, Eh and pH conditions. For our samples TVG4-1 and TVG4-2, Eu anomalies varied irregularly along the profile across the chimney wall (Figure 8). Therefore, the influence of precipitation processes on the REE pattern of our sulfide samples may be limited and needs to be studied in detail in the future.

Secondly, the negative Eu anomalies of sulfides might be the results of complexity in hydrothermal fluids and water-rock interaction processes occurred in SWIR 49°39′E field. For example, due to the geological setting of the ultraslow-spreading ridge and mixed host rocks (basalt and ultramafic rock). Moreover, the REE patterns for hydrothermal fluids are not only dependent on the water-rock interaction, but also on the compositions and tectonic setting of the fluids. At the Pacmanus field in the Manus basin, the REE patterns of anhydrites are varied often with a weak or negative Eu anomaly [36], similar to the sulfides in our study area. According to Bach et al. [37], at the Pacmanus field, the main REE complexing ligands are F^- and Cl^- in the more oxidative fluid because of the addition of gases like HF and SO_2 degassed from the mantle. This is different from the typical fields along MORs such as the TAG on the MAR, where REEs generally complex with Cl^- and OH^-. The distinct REE patterns for anhydrite can be attributed to the different complexation behavior, which is sensitive to conditions such as temperature, pressure, pH and Eh. The characteristic positive Eu anomaly for the most hydrothermal fluids should be attributed to the intense complexation of Eu^{2+} with Cl^- at high temperatures. At lower temperatures, the similar complexation behavior of Eu with other REEs results in a flat pattern with the weak Eu anomalies for this study [36]. Due to lacking of data about the temperature of fluids or sulfide precipitating in this study area, we assume that similar model could be applied in our study area. However, more efforts are needed to find evidence for the influence of the temperature on the REE composition of sulfides in the field.

4 Conclusions

The spreading rate is known to influence the location, extent and features of sulfide deposits on MORs. This paper reported our study on the first sulfide chimney samples obtained from the SWIR 49°39′E field, which is the first one found on the ultraslow-spreading ridge. The main results of our studies on mineral and geochemical compositions of

sulfides are presented as follows.

(1) The sulfide chimneys in the SWIR 49°39′E field consist mainly of pyrite and chalcopyrite and are characterized by very high metal content. Average Cu and Fe contents are 2.83% and 45.6% respectively. Concentrations of Au and Ag in the studied samples are about 2.0 ppm and 70.2 ppm respectively, higher than those find in other well known hydrothermal fields along the mid-ocean ridges.

(2) The studied chimneys show a concentric mineral zoning around the axial channel. The interior consist mainly of chalcopyrite, with pyrite and sphalerite as minor minerals. In the intermediate portion, pyrite becomes the dominant mineral, with chalcopyrite and sphalerite as minor constituents. For the outer wall, the main sulfides are pyrite and sphalerite, with chalcopyriteas minor constituent. From the inner to the outer, the mineral grains become smaller, their crystal forms become imperfect and interstices among minerals become abundant. These features are similar to those chimney edifices found from EPR and MAR.

(3) The REE geochemistry is characterized by LREE-enrichment and a weak, mostly negative, Eu anomaly. This is different from the sulfide recovered from typical fields along sediment-starved MORs. This might attribute to the distinct mineralization environment and fluid compositions in this area.

We thank DY115-19 Cruise Leg 1&2 science party who contributed to the success of this project. This work was supported by the China Ocean Mineral Resources Research and Development Association Program (*DY115-02-1-01*) *and the State Oceanic Administration Youth Science Fund* (*2010318*).

1 Corliss J B, Dymond J, Gordon L I, et al. Submarine thermal springs on the Galápagos Rift. Science, 1979, 203: 1073–1083
2 Baker E T, German C R. On the distribution of hydrothermal vent fields. In: German C R, Lin J, Parson L M, eds. Mid-Ocean Ridges: Hydrothermal interactions between the lithosphere and oceans. Geophysical Monograph, AGU, Washington, DC, 2004. 245–266
3 Banerjee R, Ray D. Metallogenesis along the Indian Ocean Ridge system. Curr Sci, 2003, 85: 321–327
4 Chen Y J, Morgan J P. The effect of magma emplacement geometry, spreading rate, and crustal thickness on hydrothermal heat flux at mid-ocean ridge axes. J Geol Res, 1996, 101: 475–482
5 Chen Y J, Lin J. Mechanisms for the formation of ridge-axis topography at slow-spreading ridges: A lithospheric-plate flexural model. Geophys J Int, 1999, 136: 8–18
6 Georgen J E, Lin J, Dick H J B. Evidence from gravity anomalies for interactions of the Marion and Bouvet hotspots with the Southwest Indian Ridge: Effects of transform offsets. Earth Planet Sci Lett, 2001, 187: 283–300
7 Muller M R, Minshull T A, White R S. Segmentation and melt supply at the Southwest Indian Ridge. Geology, 1999, 27: 867–870
8 Sauter D, Patriat P, Rommevaux-Jestin C, et al. The Southwest Indian Ridge between 49°15′E and 57°E: Focused accretion and magma redistribution. Earth Planet Sci Lett, 2001, 192: 303–317
9 Georgen J E, Kurz M D, Henry J B, et al. Low $^{3}He/^{4}He$ ratios in basalt glasses from the western Southwest Indian Ridge (10°–24°E). Earth Planet Sci Lett, 2003, 206: 509–528
10 Baker E T, Edmonds H N, Michael P J, et al. Hydrothermal venting in magma deserts: The ultraslow spreading Gakkel and Southwest Indian Ridges. Geochem Geophys Geosyst, 2004, 5: 1–24
11 German C R, Baker E T, Mevel C, et al. Hydrothermal activity along the southwest Indian ridge. Nature, 1998, 395: 490–493
12 Bach W, Banerjee N R, Dick H J B, et al. Discovery of ancient and active hydrothermal systems along the ultra-slow spreading Southwest Indian Ridge 10°–16°E. Geochem Geophys Geosyst, 2002, 3: 1044
13 Münch U, Lalou C, Halbach P, et al. Relict hydrothermal events along the super-slow Southwest Indian spreading ridge near 63°56′E-mineralogy, chemistry and chronology of sulfide samples. Chem Geol, 2001, 177: 341–349
14 Banerjee R, Dick J B H, Wolfgang B, et al. Discovery of peridotite-hosted hydrothermal deposits along the ultraslow-spreading Southwest Indian Ridge. Geol Soc Am Annu Meet, Boston, 2001. 800
15 Dick H J B, Lin J, Schouten H. An ultraslow-spreading class of ocean ridge. Nature, 2003, 426: 405–412
16 Font L, Murton B J, Roberts S, et al. Variations in melt productivity and melting conditions along SWIR (70°–49°E): Evidence from olivine-hosted and plagioclase-hosted melt inclusions. J Petrol, 2007, 48: 1471–1494
17 Cannat M, Sauter D, Mendel V, et al. Modes of seafloor generation at a melt-poor ultraslow-spreading ridge. Geology, 2006, 34: 605–608
18 Sauter D, Carton H, Meyzen C, et al. Ridge segmentation and the magnetic structure of the Southwest Indian Ridge (at 50°300′E, 55°300′E and 66°200′E): Implications for magmatic processes at ultraslow-spreading centers. Geochem Geophys Geosyst, 2004, 5: Q05K08
19 Sauter D, Mendel V, Rommevaux-Jestin C, et al. Focused magmatism versus amagmatic spreading along the ultra-slow spreading Southwest Indian Ridge: Evidence from TOBI side scan sonar imagery. Geochem Geophys Geosys, 2004, 5: Q10K09
20 Cannat M, Sauter D, Bezos A, et al. Spreading rate, spreading obliquity, and melt supply at the ultraslow spreading Southwest Indian Ridge. Geochem Geophys Geosys, 2008, 9: Q04002
21 Gautheron C E, Bezos A, Moreira M, et al. Helium and trace element geochemical signals in the southwest Indian Ridge. Goldschmidt Conference Abstracts. Geoch Cosmoch Acta, 2008, 72: A300
22 Sauter D, Cannat M, Meyzen C, et al. Propagation of a melting anomaly along the ultra-slow Southwest Indian Ridge between 46°E and 52°20′E: Interaction with the Crozet hot-spot? En révision après corrections modérées pour publication. Geophys J Int, 2009, 179: 1–22
23 Zhang T, Gao J Y, Tan Y H, et al. Effect of transform faults in the ridge-plume interaction system on the SWIR and sources of hydrothermal indications in the water column (in Chinese). Conference Abstracts of Proceedings of the 2nd Forum on Submarine Geosciences, 2007, 12
24 Muller M R, Minshull T A, White R S. Crustal structure of the Southwest Indian Ridge at the Atlantis Ⅱ Fracture Zone. J Geophys Res, 2000, 105: 25809–25828
25 Münch U, Blum N, Halbach P. Mineralogical and geochemical features of sulfide chimneys from the MESO zone, Central Indian Ridge. Chem Geol, 1999, 155: 29–44
26 Haymon R M. Growth history of hydrothermal black smoker chimneys. Nature, 1983, 301: 695–698
27 Janecky D R, Seyfried W E. Formation of massive sulfide deposits on oceanic ridge crest: Incremental reaction models for mixing between hydrothermal solutions and seawater. Geoch Cosmoch Acta, 1984, 48: 2723–2738
28 Tivey M K, Humphris S E, Thompson G, et al. Deducing patterns of fluid flow and mixing within the TAG active hydrothermal mound using mineralogical and geochemical data. J Geophys Res, 1995, 100: 12527–12555
29 Rona P A, Klinkhammer G, Nelsen T A, et al. Black smokers, massive sulfides and vent biota at the mid-ocean ridge. Nature, 1986, 321: 33–37
30 Graham U M, Bluth G L, Ohmoto H. Sulfide-sulfate chimneys on the East-Pacific Rise, 11°N and 13°N latitudes: Part I. Mineralogy and paragenesis. Can Mineral, 1988, 26: 487–504
31 Hekinian R, Fouquet Y. Volcanism and metallogenesis of axial and off-axial structures on the East Pacific Rise near 13°N. Econ Geol, 1985, 80: 221–249
32 Zeng Z G, Jiang F Q, Qin Y S, et al. Rare earth element geochemistry

of massive sulfides from the Jade hydrothermal field in the central Okinawa Trough (in Chinese). Acta Geol Sin, 2001, 75: 244–249
33 Allen D E, Seyfried W E. REE controls in ultramafic hosted MOR hydrothermal systems: An experimental study at elevated temperature and pressure. Geochim Cosmochim Acta, 2005, 69: 675–683
34 Douville E, Bienvenu P, Charlou J L, et al. Yttrium and rare earth elements in fluids from various deep-sea hydrothermal systems. Geochim Cosmochim Acta, 1999, 63: 627–643
35 Humphris S E. Rare earth element composition of anhydrite: Implications for deposition and mobility within the TAG hydrothermal mound. Proc ODP, Sci Results, 158: 143–159
36 Sverjensky D A. Europium redox equilibria in aqueous sotution. Earth Planet Sci Lett, 1984, 67: 70–78
37 Bach W, Roberts S, Vanko D A, et al. Controls of fluid chemistry and complexation contents of anhydrite from the Pacmanus subseafloor hydrothermal system, Manus Basin, Papua New Guinea. Mineral Deposit, 2003, 38: 916–935
38 Marchig V, Blum N, Roonwal G. Massive sulfide chimneys from the East pacific Rise at 7°24′S and 16°34′S. Mar Geores Geoth, 1997, 15: 49–66
39 Bogdanov Y, Gurich E, Kuptsov V, et al. Relict sulfide mounds at the TAG hydrothermal field of the Mid-Atlantic Ridge (26°N, 45°W). Oceanology, 1995, 34: 534–542
40 Halbach P, Pracejus B, Maerten A. Geology and mineralogy of massive sulfide ores from the central Okinawa Trough, Japan. Econ Geol, 1993, 88: 2210–2225